Pre-publication version
J.Y. Ho et al. International Journal of Heat and Mass Transfer 150 (2020) Article 119262
https://doi.org/10.1016/j.ijheatmasstransfer.2019.119262

Additively-manufactured metallic porous lattice heat exchangers for air-side heat transfer enhancement

J.Y. Ho, K.C. Leong*, T.N. Wong
Singapore Centre for 3D Printing, School of Mechanical and Aerospace Engineering, Nanyang Technological University, 50 *Nanyang Avenue, Singapore* 639798*, Republic of Singapore*

ABSTRACT

In this study, two novel porous lattice air-cooled heat exchangers (Lattice 1 and Lattice 2) were fabricated by the selective laser melting (SLM) technique from an aluminum alloy (AlSi10Mg) powder. Repetitions of the Rhombi-Octet unit cells of different cell sizes were used to form the porous matrices. Experiments were carried out in a wind tunnel to evaluate the thermal-hydraulic performances of the heat exchangers. The thermal performance indicators such as the overall thermal conductance (UA), air-side thermal resistance (R_a), air-side heat transfer coefficient (h_a) and volumetric heat flux density ($\dot{q}_v$) of the porous lattice heat exchangers were determined and comparisons were made against two conventional fin-tube heat exchangers (Fin-tube 1 and Fin-tube 2). In addition, the pressure drops across the heat exchangers were also measured. Based on our investigations, it was determined that Lattice 1 exhibited approximately 40% - 45% higher UA and h_a than Lattice 2. However, the pressure drop across Lattice 1 was also higher than Lattice 2. At the same mass flow rate of air ($\dot{m}_a$), it was found that the h_a values of the porous lattice heat exchangers were more than 2 times those of the fin-tube heat exchangers. The significantly higher h_a values of the porous lattice are mainly attributed to the presence of interconnected pores and the formation of eddies downstream of the ligaments that improved fluid mixing. For the same pumping power ($\dot{W}/H$), the use of the porous lattice heat exchangers also resulted in consistently higher h_a values than the fin-tube heat exchangers. These results demonstrated the potential of using SLM to fabricate a new generation of commercial-scale compact heat exchangers made of porous lattices. These new porous lattice structures have enhanced the thermal performances of the heat exchanger with no penalty in pumping power.

KEYWORDS: additive manufacturing; selective laser melting; porous lattice; air-cooled; heat exchanger

1. Introduction

Air-cooled heat exchangers are widely used in many industrial systems such as those found in the building HVAC (heating ventilation and air-conditioning) units, power plants and automotive coolers. However, due to the poor thermophysical properties of air, the air-side convection resistance is usually the dominant resistance of an air-cooled heat exchanger. To improve the air-side heat transfer coefficient, the use of enhanced surfaces has been widely explored. In the past few decades, conventional finned surfaces such as wavy fins, slit fins, louvered fins and fins with vortex generators [1 – 7] have been developed to enhance the air-side heat transfer coefficients with relative success. Vortex shedding, boundary layer reset and improved fluid mixing are some of the heat transfer enhancement mechanisms suggested. However, due to the limitation in conventional fabrication techniques, these heat exchangers are largely limited to fin-and-tube designs. In view of their widespread applications, heat exchangers with higher heat transfer coefficients, lower pressure drops and low production costs are needed to improve the system energy efficiency and to better cope with the global demand.

In this regard, the recent advancements in additive manufacturing (AM) have enabled the fabrication of heat exchangers with new and complex designs. In AM, a solid material is added layer-by-layer to form a three-dimensional object in accordance to a pre-programmed computer-aided design (CAD) model. This manufacturing method allows the freedom of producing complex three-dimensional structures that are otherwise challenging or impossible to be fabricated by conventional manufacturing techniques. Selective laser melting (SLM) and direct laser sintering (DLS) are AM techniques which allow metallic components to be

* Corresponding author: mkcleong@ntu.edu.sg

fabricated. Due to this advantage, there has been an increasing interest in exploring the use of SLM and DLS to produce functional metallic components for heat transfer applications in the recent years. Fasano et al. [8] fabricated two air-cooled heat sinks by SLM that consist of a combination of hollow fins, a static pressure plug and openings on the fin structures. These heat sink designs aim to induce secondary flow within the fins. From their experimental results, it was shown that up to 95% enhancement in air-side thermal conductance could be achieved as compared to a conventional longitudinal-fin heat sink. Microchannels with different pin fin spacings were fabricated by Kirsch and Thole [9] using the Laser Power Bed Fusion technique. It was determined that the microchannel with the fewest pin fins exhibited similar Nusselt numbers as compared to the microchannel with more than six times the number of pin fins. It was concluded that substantial weight reduction can be achieved by using fewer pin fins. On the other hand, Son et al. [10] investigated the forced convection heat transfer performance of periodically-arranged tetrahedral lattice unit cell structures. The structures were fabricated by AM and it was shown that these lattice frames provided the benefit of high porosity and surface area-to-volume ratio while displaying lower pressure drops and high structural integrity. More recently, an additively manufactured lattice heat sink was also investigated by Alexandersen et al. [11] for passive air cooling of light-emitting diode (LED) lamps. However, it was determined from their numerical studies that the base temperature of the lattice heat sink was higher than the topology optimized and pin fin structures.

Nomenclature

A	area (m^2)	t	tube thickness (m)
A_a	total air-side surface area (m^2)	T	temperature (ºC)
A_c	minimum cross-sectional free flow area (m^2)	U	overall heat transfer coefficient ($W/m^2 \cdot K$)
A_p	surface area of porous lattice (m^2)		
C_p	specific heat (J/kg·K)	u	velocity (m/s)
D_h	hydraulic diameter (m)	V	volumetric flow rate (m^3/s)
d_o	outer tube diameter (m)	Vol	volume of heat exchanger (m^3)
F	correction factor	W	width of heat exchanger (m)
f_p	fin pitch (m)	$\dot{W}$	pumping power (W)
f_t	fin thickness (m)	Z_T	transverse tube pitch (m)
h	heat transfer coefficient ($W/m^2 \cdot K$)	Z_L	longitudinal tube pitch (m)
H	depth of heat exchanger (m)		
k_a	thermal conductivity of air (W/m·K)	β	surface area-to-volume ratio
k_{eff}	effective thermal conductivity (W/m·K)	ρ	density (kg/m^3)
k_f	thermal conductivity of aluminum fin (W/m·K)	η_a	overall surface efficiency
L	length of heat exchanger (m)	η_f	fin efficiency
$LMTD$	log mean temperature difference (K)	μ_f	dynamic viscosity (kg/m·s)
L_p	height of porous fin (m)		
$\dot{m}_a$	mass flow rate of air (kg/s)	*Subscripts*	
Nu	Nusselt number	a	air-side
ΔP	pressure drop (kPa)	w	water-side
Q	heat rate (W)	in	inlet
$\dot{q}_v$	volumetric heat flux density ($W/m^3 \cdot K$)	out	outlet
r_c	fin collar radius outer radius (m)	$cond$	conduction
R	thermal resistance (K/W)		
Re	Reynolds number		

In the recent years, AM has also been used to fabricate a new generation of innovative heat exchangers that involved more than one working fluid for various engineering applications. For instance, Arie et al. [12, 13] designed and fabricated air-to-liquid cross-flow heat exchangers that consist of a hybrid of manifolds and microchannels for air-side heat transfer enhancement. The designs aim to reduce the airflow length and thereby

maintain the flow in the developing region. The heat exchangers were designed for dry cooling of power plants and the DLS technique was employed to fabricate the heat exchangers. It was reported that the manifold-microchannel heat exchangers had better thermal performance as compared to conventional wavy, plain plate, louvered fin heat exchangers but were poorer in performance than the strip fin heat exchanger. Subsequently, Zhang et al. [14] adopted the manifold-microchannel design and fabricated a gas-to-gas heat exchanger. They demonstrated the use of this AM-fabricated heat exchanger for high temperature conditions. On the other hand, Unger et al. [15] experimentally investigated the thermal-hydraulic performances of two new annular fin designs fabricated by SLM. The designs consist of pin fins integrated in circular (CIPF) and serrated (SIPF) annular fins. They suggested that such designs improve heat conduction from the fin base to the fin tip. From their experimental investigation, it was determined that the highest volumetric heat flux density of 2.72 $kW/m^3 \cdot K$ was achieved with the SLM fabricated circular integrated pin fins (CIPF). More recently, a new type of cross flow heat exchanger with inter-layer flow conduits, fabricated by SLM, was reported by Greiciunas et al. [16]. The thermal-hydraulic performances of the heat exchanger were numerically evaluated. The heat transfer performances of the inter-layer heat exchanger were found to be 7% - 13% higher than the conventional pin-fin heat exchanger with no penalty in pressure drop.

Apart from the fabrication of small-scale heat exchangers, several investigations have also been made on the use of AM to produce larger commercial-scale air-cooled heat exchangers. For example, Hathaway et al. [17] designed and investigated a plate-fin and tube air-cooled heat exchanger for the cooling of hydraulic oil in a commercial excavator. The heat exchanger of dimensions 430 × 530 × 50 mm consists of inlet and outlet manifolds, tubes, internal and external features. It was fabricated as one integrated part using SLM. On the other hand, Saltzman et al. [18] additively manufactured two full-scale air-cooled heat exchangers for aircraft oil cooling application. These AM heat exchangers have similar sizes as the conventionally manufactured plate-fin oil coolers. The initial temperature difference normalized heat rejection rate of the heat exchanger (W/ITDc) was used as the thermal performance evaluation criterion. Based on this evaluation criterion, it was found that the thermal performance of the AM heat exchangers was about 10% higher than the conventionally manufactured ones. However, the air-side pressure drop was approximately twice as large. From the above brief review, it can be seen that there has been relative success in employing AM to produce functional air-cooled heat exchangers. However, only marginal thermal enhancements were achieved with the AM-produced heat exchangers as compared to conventional heat exchangers. This provides the motivation for further developments of new heat exchanger designs to enhance the air-side heat transfer coefficient.

One possible method of enhancing the air-side heat transfer is by employing metallic porous media such as the aluminum foam [19, 20]. These porous matrices have large specific areas, are light and are able to induce fluid mixing which promotes heat transfer. These key features have rendered them suitable for cooling applications such as in electronic devices, and in the aerospace, automobile and defense industries [21, 22]. For air-cooled heat exchanger investigations, T'Joen et al. [23] studied the air-side heat transfer rate of circular tube heat exchangers covered with aluminum foam on the external tube wall. It was reported that the thermal performances of the aluminum foam heat exchangers were higher than the conventional helical finned tube heat exchangers when the bonding resistance between the metallic foam and the tube wall was reduced by an appropriate brazing process. Chumpia and Hooman [24, 25] investigated the thermo-hydraulic performances of tubular aluminum foam heat exchangers of different foam thickness in a wind tunnel facility. The experimental results of the aluminum foam heat exchangers were compared against conventional circular fin heat exchangers. It was found that even though the increase in aluminum foam thickness reduces the total thermal resistance, it also increases the pressure drop across the heat exchangers. In addition, their results also concluded that at the same pressure drop, an aluminum foam heat exchanger has higher heat transfer rate as compared to a conventional circular fin heat exchanger. Nawaz et al. [26, 27] explored the use of aluminum foams as compact heat exchangers for the replacement of conventional fin heat exchangers. The heat exchangers have a face area of 200 × 200 mm^2 and consist of 10 layers of aluminum foams bonded onto the external walls of the flat tubes. A detailed parametric study was carried out to characterize the thermal-hydraulic performances of the metallic foams with different pore sizes. Dai et al. [28] compared the heat transfer and pressure drop characteristics of an aluminum foam heat exchanger and a conventional louvered fin heat exchanger. The aluminum foam heat exchanger was found to have the same heat transfer rate as the

louvered fin heat exchanger but at a lower volume and weight. However, the cost of producing the aluminum foam heat exchanger was significantly higher. Recently, a new type of porous medium, viz., the periodic lattice structure, was investigated by Ho et al. [29 – 31] for enhancing the thermal-hydraulic performances of water-cooled cold plates and air-cooled heat sinks. The lattice structure, produced by SLM, consists of orderly arrangements of the Rhombi-Octet unit cell. Due to its ligament arrangements, this unit cell design has higher packing density and lower porosity than the aluminum foams. From the experimental investigation, the lattice structure exhibited up to 383% enhancement in the heat transfer coefficient as compared to an empty channel and up to 51% enhancement as compared to conventional twisted tape inserts [29]. Furthermore, it was also determined that the lattice structure demonstrated higher effective thermal conductivity and heat transfer rate than the aluminum foam [28, 29]. In addition, due to the orderly arrangement of the unit cells, the lattice structures also have similar or better hydraulic performances than the aluminum foams [30, 31].

Due to the promising thermal-hydraulic performances of the Rhombi-Octet lattice structure, this paper seeks to extend our previous studies by exploring the possibility of fabricating and characterizing two commercial-scale air-cooled porous lattice heat exchangers. The porous lattice heat exchangers, consisting of different Rhombi-Octet unit cell sizes, were fabricated by SLM. Experiments were conducted in a wind tunnel test facility and a hot water circulation loop to evaluate the heat transfer and pressure drop performances of the heat exchangers. In addition, comparisons were made against two conventional fin-tube heat exchangers. Based on the results obtained, the possible heat transfer mechanisms were identified and the best heat exchanger design was selected.

2. Design and fabrication of heat exchangers

The design of the lattice porous heat exchanger that is employed in the present investigation is depicted in Fig. 1. The heat exchanger has a face area of 215 mm × 180 mm. It consists of 10 parallel water flow channels with each pair of flow channels connected to common inlet and outlet headers. Each flow channel has an internal cross-sectional area of 4 mm × 80 mm and a wall thickness of 2 mm. The flow channels are 14 mm apart and the porous lattices are located between the void spaces of the flow channels. The lattice structure consists of repetitions of the Rhombi-Octet unit cells which are periodically arranged to form a porous matrix. The drawing of a Rhombi-Octet unit cell is shown in Fig. 2. A detailed explanation of the unit cell geometry is provided in Refs. [29, 31]. The unit cell consists of 18 square and 24 triangular faces and examples of the square and triangular faces are highlighted in blue and red, respectively in Fig. 2. Each square is positioned at 45° to its adjacent squares to form a Rhombicuboctahedron core whereas at each corner, the triangles are arranged to form an Octet truss-like structure. Each unit cell has the dimensions of ω on all sides. In this study, two porous lattice heat exchangers were fabricated. One heat exchanger is made of repetitions of unit cells with ω = 7 mm whereas the other heat exchanger consists of unit cells with ω = 14 mm. The specifications of the porous lattice heat exchangers are summarized in Table 1. It should be noted that the fin height (L_p) of the porous lattice is taken as half the distance between two flow channels. On the other hand, β and k_{eff} are the surface area-to-volume ratio and effective thermal conductivity of the lattice structures, respectively. The relationships between β, k_{eff} and the lattice structure unit cell size were previously established by Ho et al. [31]. Their values were computed and presented in Table 1.

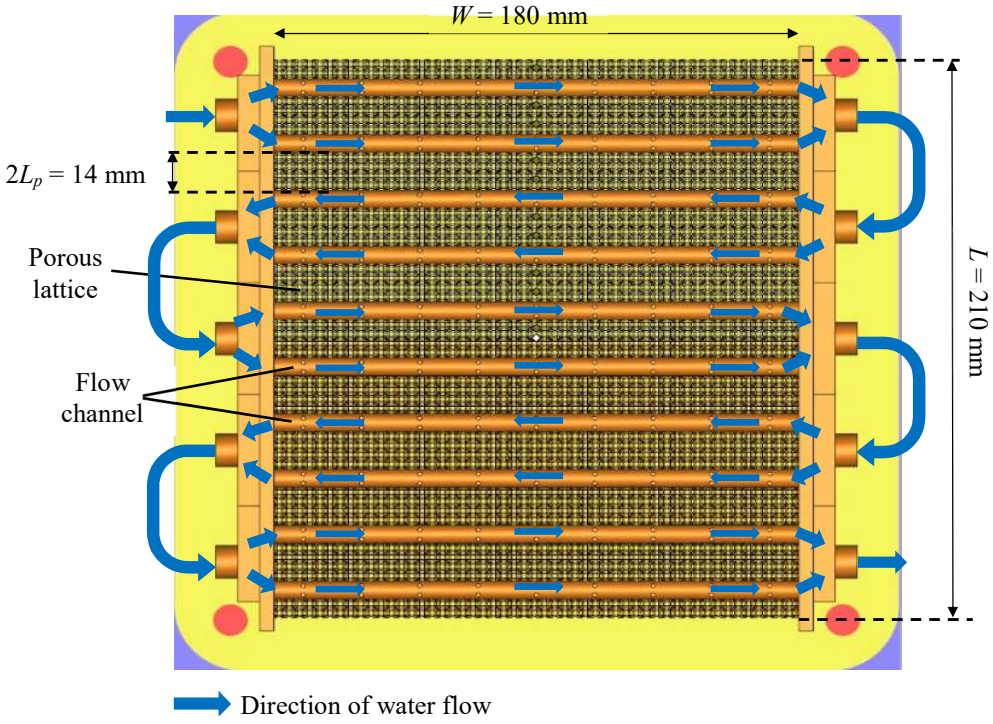

Fig. 1 Porous lattice heat exchanger design (top view).

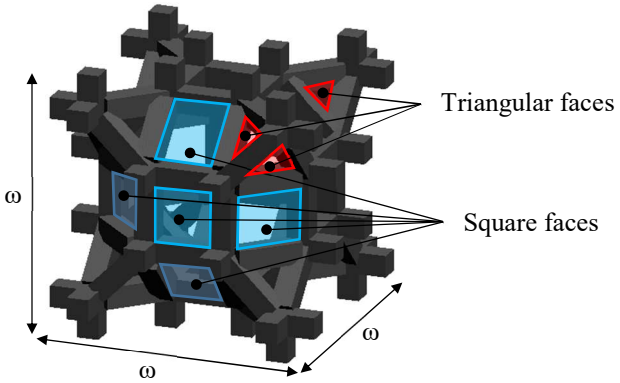

Fig. 2 Schematic of Rhombi-Octet lattice unit cell.

Table 1 Specifications of SLM fabricated porous lattice heat exchangers

Porous lattice heat exchanger	Lattice 1	Lattice 2
Face area of heat exchanger ($L \times W$) [mm]	210 × 180	210 × 180
Depth of heat exchanger (H) [mm]	80	80
Fin height (L_p) [mm]	7	7
Lattice structure unit cell size (ω) [mm]	7	14
Total surface area (A_a) [m^2]	2.204	1.275
Surface area-to-volume ratio (β) [m^{-1}]	968	470
Effective thermal conductivity of lattice structure(k_{eff}) [W/m·K]	19.04	14.56
Material	AlSi10Mg	

The porous lattice heat exchangers were fabricated using the SLM 250 HL (SLM Solutions GmbH) facility at the Future of Manufacturing Laboratory 1 of the Singapore Centre for 3D Printing (SC3DP) in Nanyang Technological University (NTU), Singapore. The machine utilized a Gaussian distributed Yb:YAG laser with maximum power of 400 W and laser beam spot size of 80 μm to melt and fuse the base metallic powder. An aluminum alloy powder (AlSi10Mg) of 20 μm to 63 μm size distribution was employed as the base metallic powder to fabricate the heat exchanger for the experiments. The aluminum alloy (AlSi10Mg) was selected as it has relatively high thermal conductivity and is light as compared to other common metals such as iron, stainless steel and titanium. The material composition of AlSi10Mg has also been optimized for the additive manufacturing process and thus enables bulk materials with good structural strength and hardness to be produced. The laser melting process was carried out in the machine's build chamber. Prior to the start of the fabrication process, inert argon gas was first used to flush the chamber to attain an oxygen level of less than 0.2% so as to minimize oxidation and combustion of powder. Subsequently, the first layer of AlSi10Mg metallic powder was distributed evenly on the base-plate by a recoater. The laser beam was then directed to melt the powder based on a preprogrammed model. Upon completion of the laser melting process for the first layer, the base-plate was then lowered by one-layer thickness of 50 μm and the process was repeated until the parts are fully constructed. In the present investigation, a laser power of 200 W, scanning speed of 1300 mm/s and hatching spacing of 0.08 mm were used to fabricate the heat exchangers. The fabricated Lattice 1 heat exchanger is shown in Fig. 3. It can be seen that some artificial structures were designed and fabricated with the heat exchanger. These artificial structures were included to support some regions of the porous lattice fins and circular tubes of the heat exchanger. This prevented any overhanging features during the laser melting process and thus minimized the fabrication defects and failures. It can also be seen in Fig. 3 that the heat exchangers were fabricated onto an aluminum base plate. After the SLM process was completed, electrical discharge machining (EDM) was used to separate the heat exchanger from the base plate. In addition, the excess artificial structures on the heat exchanger were also removed.

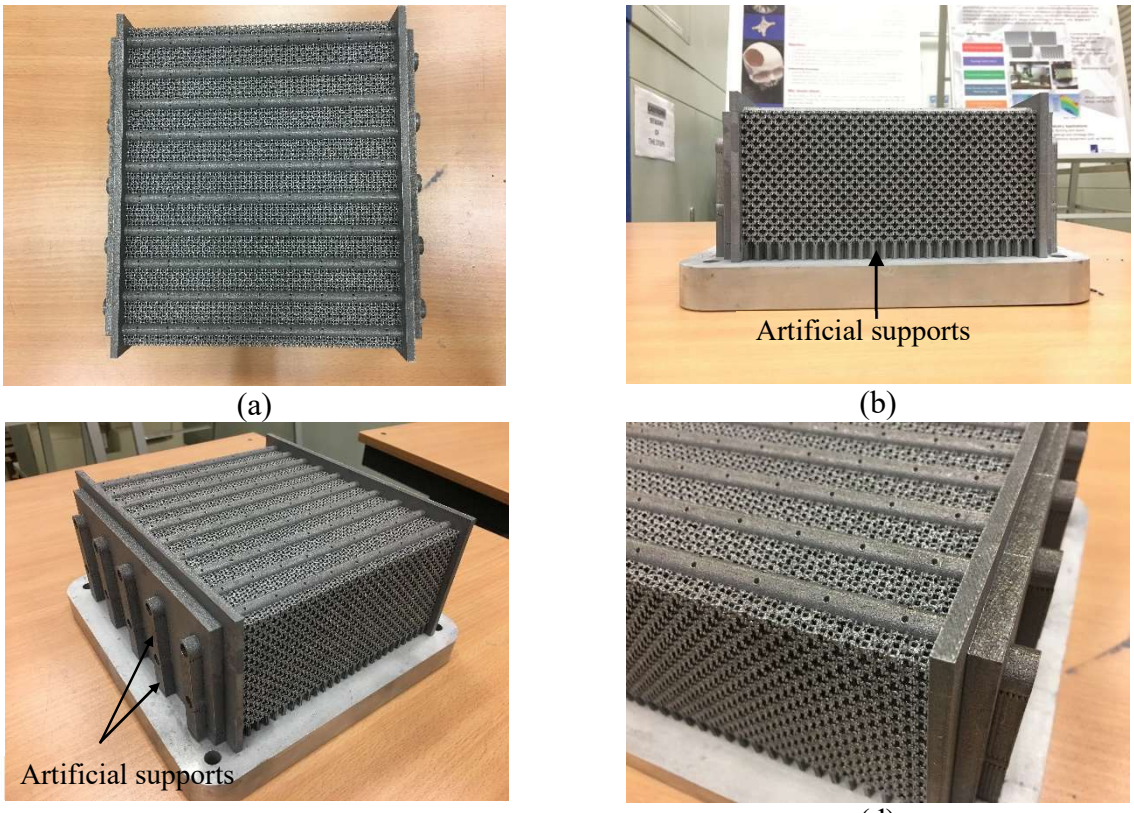

Fig. 3 Images of fabricated Lattice 1 heat exchanger (a) top view, (b) side view, (c) isometric view and (d) zoom-in view.

Two conventional fin-and-tube cross flow heat exchangers (Fin-tube 1 and Fin-tube 2) were also prepared and experimentally investigated. These heat exchangers were purchased commercially. They are made of arrays of horizontal copper tubes with an outer diameter of 9.7 mm and tube thickness of 0.5 mm. Aluminum wavy fins with the thickness of 0.1 mm are arranged perpendicular to the horizontal tubes. During the experiments, hot water was directed through the internal flow channel of the copper tubes whereas air flows over the aluminum wavy fins and the external tube surface. An image of Fin-tube 1 is shown in Fig. 4 and the symbols indicating its bulk dimensions are also shown in this figure. The various geometric parameters of the conventional fin-and-tube heat exchangers are presented in Table 2. It should be noted that, for both Fin-tube 1 and Fin-tube 2, the tube arrays are in staggered arrangement.

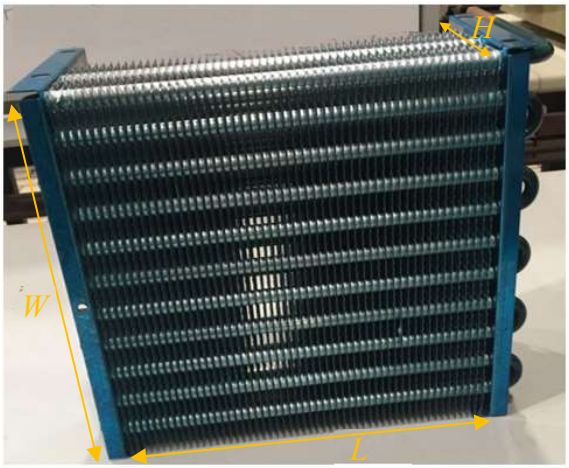

Fig. 4 Image of Fin-tube 1 heat exchanger.

Table 2 Specifications of conventional fin-and-tube heat exchangers

Fin-and-tube heat exchanger	Fin-tube 1	Fin-tube 2
Face area of heat exchanger ($L \times W$) [mm]	280 × 280	214 × 204
Depth of heat exchanger (H) [mm]	88	60
Fin pitch (f_p) [mm]	5.1	2.9
Fin thickness (f_t) [mm]	0.1	0.1
Tube outer diameter (d_o) [mm]	9.7	9.7
Tube wall thickness (t) [mm]	0.5	0.5
Traverse tube pitch (Z_T) [mm]	25.5	25.5
Longitudinal tube pitch (Z_L) [mm]	22	20
No of tube rows	4	3
Total surface area (A_a) [m^2]	2.96	1.85
Material	Aluminum fins and copper tubes	

3. Experimental setup and procedures

The experimental setup employed for the heat transfer and pressure drop investigation is shown in Fig. 5. It consists of an open-loop wind tunnel and a closed-loop hot water circulation system. The wind tunnel consists

of a contraction cone section and air duct constructed from fiberglass. The airflow and air temperature measurement stations, made from acrylic, are installed before and after the heat exchangers. In order to deliver the required airflow through the heat exchanger, a centrifugal fan was installed at the end of the wind tunnel. The quality of flow in the wind tunnel depends largely on the profile of the contraction cone located upstream of the flow [32, 33]. The contraction cone was designed to ensure uniform, parallel and steady flow with low turbulence level at the contraction cone outlet so that accurate measurements of the air velocity can be obtained. In this investigation, the potential flow theory was employed to develop the contraction profile based on the method described by Lam and Pomfret [33]. In addition, at the inlet of the contraction cone, a honeycomb structure and wire meshes of different cell sizes were installed to minimize the vertical velocity component in the airflow as a result of the swirling motion of air during entry. Following the construction of the wind tunnel, the air velocity at the outlet of the contraction cone was measured to determine the uniformity of the airflow. The measurements were obtained using a hot wire anemometer which has an accuracy of ±0.5% of its full-scale value of 15 m/s. The measurements were performed in accordance to ASHRAE Standard [34] where a total of 25 measurement points were taken at each fan speed and the locations of these measurements points are shown in Fig. 6(a). The measurement results are shown in Fig. 6(b) where it can be seen that the air velocities are uniform. The standard deviations between the local (U_a) and the average velocities ($U_{a,ave}$) ranged from 1.02% to 2.70%. In addition, similar measurement points and locations were also employed at the air temperature measurement station. The average temperatures were computed which gives the outlet air temperature ($T_{a,out}$).

On the other hand, the hot water system consists of a water pump and a hot water tank. The hot water tank has a storage capacity of 400 liters and was installed with an 8 kW heater. The heater was connected to a temperature controller. Based on the feedback from the thermocouples in the hot water tank, the power supplied to the heater was automatically varied to maintain a constant water temperature. The water pump was capable of delivering the water flow rate of up to 0.000117 m^3/s (or 7.0 L/min) and a variable speed drive was installed to allow the water flow rate to be controlled. Finally, a variable area flowmeter and two thermocouples were installed to determine the water flow rate (V_w) and the inlet ($T_{w,in}$) and outlet ($T_{w,out}$) water temperatures.

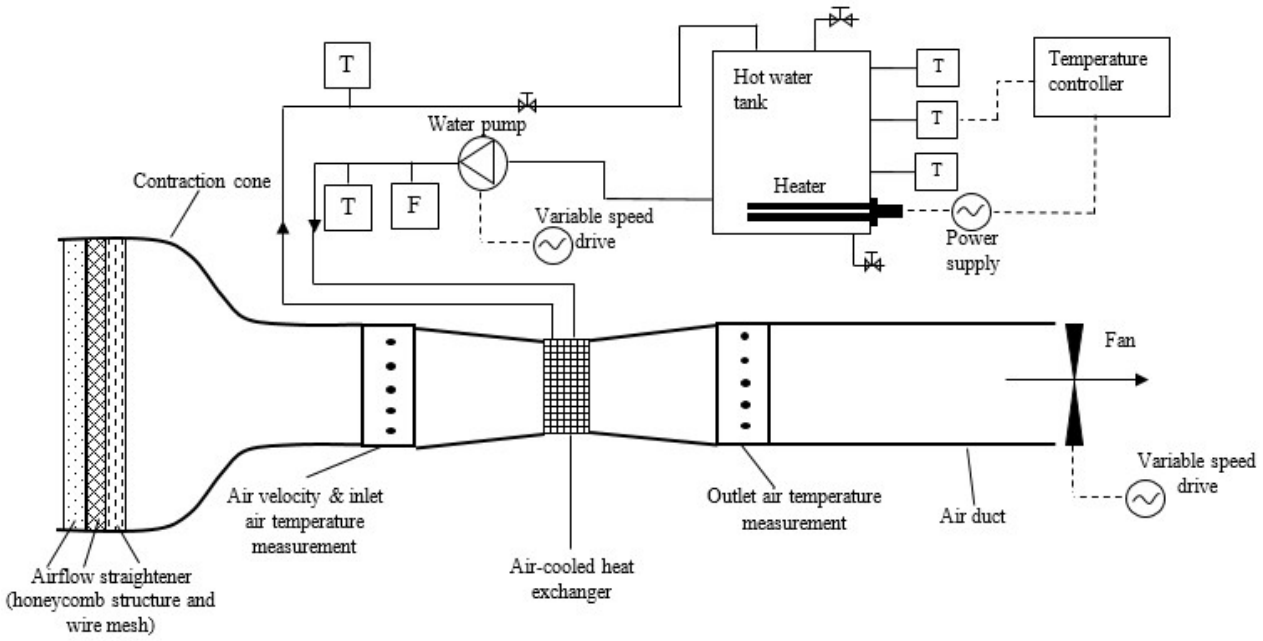

Fig. 5 Schematic of experimental setup.

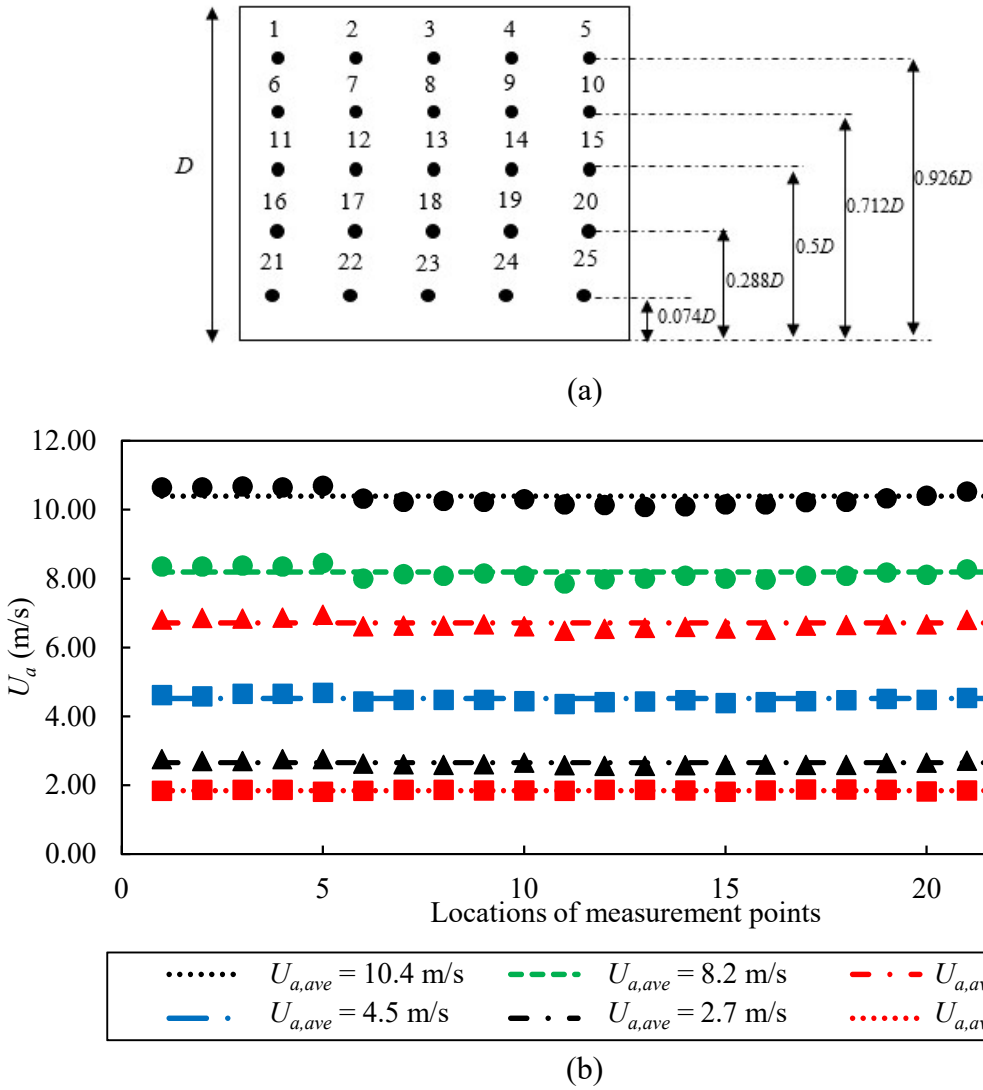

Fig. 6 (a) Air velocity and temperature measurement points and (b) air velocity measurement results.

The air-side and water-side heat transfer rates were determined from Eqs. (1) and (2), respectively. During the experiments, the temperature difference between the inlet and outlet of each fluid was kept sufficiently large in order to minimize the uncertainties of Q_a and Q_w. In addition, from the experimental results it was found that differences between Q_a and Q_w were not more than 5%. Using the log mean temperature difference (*LMTD*) method and the average values of Q_a and Q_w, the overall thermal conductance of a heat exchanger (*UA*) was computed by Eq. (4) where *LMTD* was determined by Eq. (5) and *F* denotes the correction factor. Based on the flow configuration of the porous lattice heat exchanger, *F* was estimated from Ref. [35] with the air-side as mixed flow and water-side as unmixed flow. With *UA* known, the air-side thermal resistance (R_a) was computed from Eq. (6) where R_{cond} is the heat conduction resistance across the flow channel wall, h_w is the water-side heat transfer coefficient and A_w is the area of the internal flow channel wall. The thickness of the flow channel wall is 2 mm and the thermal conductivity of the bulk AlSi10Mg (k_s) is 153 W/m·K [31]. Using these values, R_{cond} can be determined. On the other hand, the values of h_w were determined using the Wilson plot method as described in Ref. [36].

$$Q_a = \rho_a V_a C_{p,a}\left(T_{a,out} - T_{a,in}\right) \quad (1)$$

$$Q_w = \rho_w V_w C_{p,w}\left(T_{w,in} - T_{w,out}\right) \quad (2)$$

$$Q = (Q_a + Q_w)/2 \quad (3)$$

$$UA = \frac{Q}{F \cdot LMTD} \tag{4}$$

$$LMTD = \frac{(T_{w,in} - T_{a,out}) - (T_{w,out} - T_{a,in})}{ln\frac{(T_{w,in} - T_{a,out})}{(T_{w,out} - T_{a,in})}} \tag{5}$$

$$R_a = \left[\frac{1}{UA} - \frac{1}{h_w A_w} - R_{cond}\right] \tag{6}$$

The air-side thermal resistance (R_a) is related to the overall surface resistance (η_a), the air-side heat transfer coefficient (h_a) and the total surface area of the heat exchanger that is exposed to the flowing air (A_a), given by Eq. (7). In addition, η_a can be expressed by Eq. (8) where η_f and A_p represent the lattice structure fin efficiency and surface area, respectively. Following Nawaz et al. [27] and Dai et al. [28], η_f was calculated by assuming a straight fin with an adiabatic fin tip, given by Eqs. (9) and (10). In these equations, β, k_{eff} and L_p are the surface area-to-volume ratio, effective thermal conductivity and half-thickness of the lattice structures, respectively and are given in Table 2. By substituting Eqs. (8) – (10) into Eq. (7), the air-side heat transfer coefficients (h_a) were determined. Finally, it should also be noted that the pressure drops across the heat exchangers (ΔP) were also measured using the inclined manometers.

$$R_a = \frac{1}{\eta_a h_a A_a} \tag{7}$$

where

$$\eta_a = 1 - \left[A_p(1 - \eta_f)/A_a\right] \tag{8}$$

$$\eta_f = \tanh(m_p L_p)/(m_p L_p) \tag{9}$$

$$m_p = \sqrt{h_a \beta / k_{eff}} \tag{10}$$

For each heat exchanger, experiments were conducted at least twice to ensure that the results are repeatable. The thermocouples were calibrated to an accuracy of ± 0.25°C whereas the variable area flowmeter has an accuracy of ± 0.1 L/min. Due to the wide range of ΔP measured in the present investigation, inclined manometers of different range scales were used. For the measured ΔP of between 0 Pa and 500 Pa, the inclined manometer has an accuracy of ±10 Pa. On the other hand, for the measured ΔP of between 500 Pa and 1000 Pa and between 1000 Pa and 5000 Pa, the accuracies of the inclined manometers are ±20 Pa and ±100 Pa, respectively. Using the method by Moffat [37], the uncertainties of UA and h_a were determined to be between ± 4% and ± 8%.

4. Results and discussions

4.1 Heat transfer characteristics

The overall thermal conductance values (UA) of the porous lattice heat exchangers (Lattice 1 and Lattice 2) are shown in Fig. 7, where the abscissa represents the mass flow rate of air ($\dot{m}_a$). It should be noted that throughout the experiments, the volumetric flow rate of water through both heat exchangers was maintained at 5×10^{-5} m^3/s (or 3.0 L/min). Therefore, the change in UA values are mainly due to the change in $\dot{m}_a$. It can be seen from Fig. 7 that UA increases with the increase in $\dot{m}_a$. For example, for Lattice 1, UA is 168.9 W/K at $\dot{m}_a$ of 0.17 kg/s. With the increase in $\dot{m}_a$ to 0.27 kg/s, UA of Lattice 1 increases by 32% to 223.3 W/K. In addition, it can also be observed from Fig. 7 that the thermal performances of Lattice 1 are consistently higher than Lattice 2. For instance, at $\dot{m}_a$ of 0.27 kg/s, the UA value of Lattice 2 is 157.2 W/K. In comparison, at the same air mass flow rate, the UA value of Lattice 1 is about 42% higher than that of Lattice 2.

By employing Eqs. (4) – (6), the air-side thermal resistances (R_a) of the porous lattice heat exchangers were computed and compared in Fig. 8. The use of R_a eliminates the influence of the water-side heat transfer

coefficient and allows only the air-side thermal performance of the heat exchanger to be compared. It can be seen from Fig. 8 that the R_a values of Lattice 1 are significantly smaller than Lattice 2, hence, indicating that Lattice 1 has better air-side heat transfer performance. It should be noted that both the unit cells of Lattice 1 and Lattice 2 have the same porosity of 0.85. However, as shown in Table 1, Lattice 1 has a larger surface area-to-volume ratio (β) as compared to Lattice 2. This resulted in Lattice 1 having approximately 73% larger surface area that is exposed to the flowing air as compared to Lattice 2. Hence, the air-side thermal resistance of Lattice 1 is reduced.

Figure 9 shows the air-side heat transfer coefficients (h_a) of the porous lattice heat exchangers that were computed by Eqs. (8) – (10). It should be noted that h_a is computed by normalizing R_a by the total heat transfer area (A_a). This, therefore, eliminates the influence of heat transfer area on the thermal performance of the heat exchangers. It can be seen from Fig. 9 that the h_a values of both heat exchangers are similar at a low $\dot{m}_a$ of 0.17 kg/s. However, with the increase in $\dot{m}_a$, the h_a values of Lattice 1 increase more significantly than Lattice 2. For example, at a higher $\dot{m}_a$ of 0.27 kg/s, the h_a value of Lattice 1 is approximately 40% higher than Lattice 2. As shown in Fig. 2, the Rhombi-Octet unit cell has a larger void volume in its core. Therefore, air flowing through the unit cell is analogous to flowing through an expansion and contraction channel, i.e., an expansion channel when air is flowing into the unit cell and a contraction channel when it is flowing out of the unit cell. Since Lattice 1 is made of a smaller unit cell size, more repetitions of unit cells are required to form the porous matrix as compared to Lattice 2. Therefore, the air flowing through Lattice 1 may have experienced more repetitions of expansion and contraction than Lattice 2. This phenomenon may have improved fluid mixing and enhanced the heat transfer coefficient (h_a).

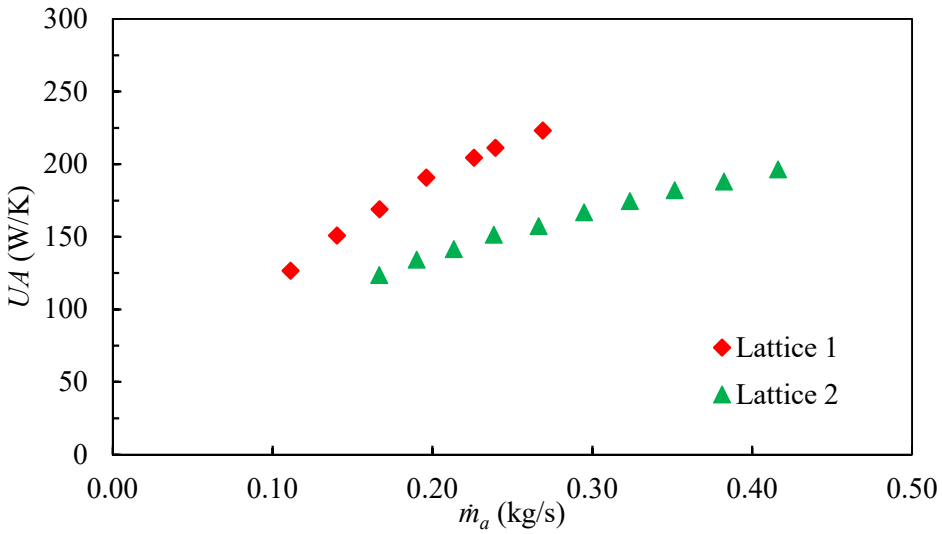

Fig. 7 Comparison of overall thermal conductances (UA) of porous lattice heat exchangers.

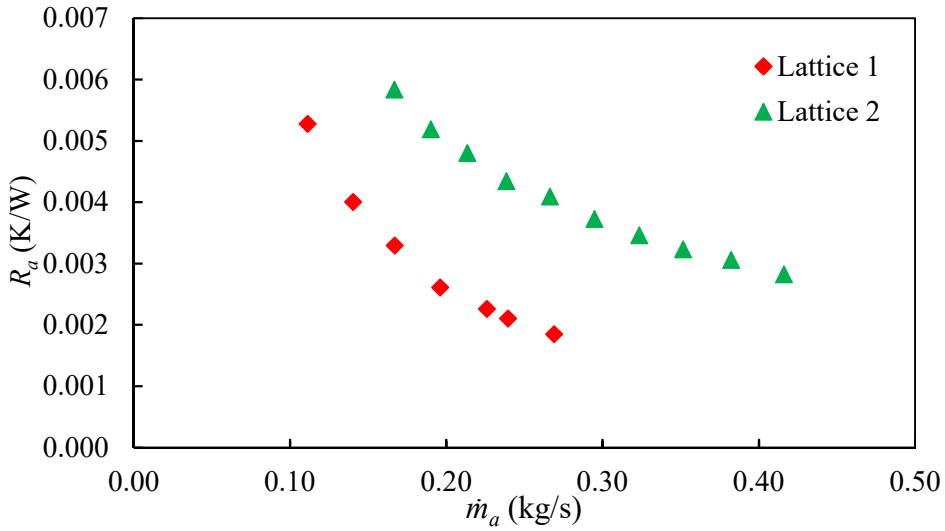

Fig. 8 Comparison of air-side thermal resistances (R_a) of porous lattice heat exchangers.

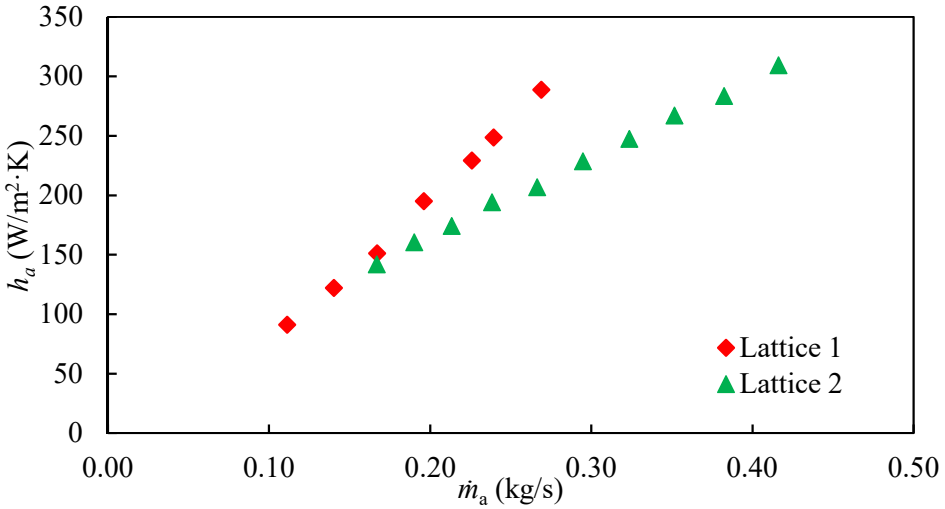

Fig. 9 Comparison of air-side heat transfer coefficients (h_a) of porous lattice heat exchangers.

4.2 Pressure drop characteristics

Fig. 10 shows the pressure drop per unit depth ($\Delta P/H$) across the porous lattice heat exchangers. Even though the Rhombi-Octet unit cells of both exchangers have the same porosity, $\Delta P/H$ of Lattice 1 is higher than that of Lattice 2. For instance, at $\dot{m}_a$ of 0.24 kg/s, Lattice 1 has a pressure drop of 0.060 kPa/mm whereas the pressure drop of Lattice 2 is only 0.028 kPa/mm. The $\Delta P/H$ value of Lattice 1 is 2.14 times that of Lattice 2. The reduction in pressure drop across the porous lattice with increasing unit cell size was similarly observed by Ho et al. [29, 31]. This is mainly attributed to the increase in the average pore diameter (d_p) of the lattice structure with increasing unit cell size. It should be noted that d_p is calculated by taking the area-weighted average of all the pores in their projected views. Since d_p of Lattice 2 is larger, its resistance to the fluid flow path reduces and therefore resulted in lower $\Delta P/H$ values.

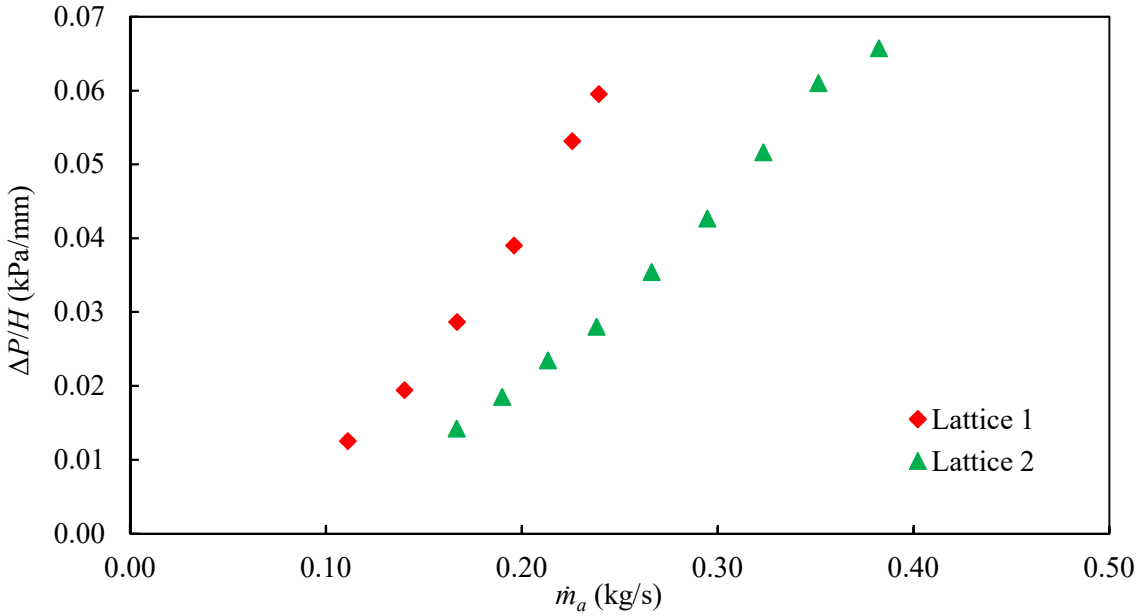

Fig. 10 Air-side pressure drop per unit depth ($\Delta P/H$) across porous lattice heat exchangers.

4.3 Comparison with conventional heat exchangers

In this section, the thermal-hydraulic performances of the SLM fabricated porous lattice heat exchangers are compared against the conventional fin-tube heat exchangers. The specifications of the fin-tube heat exchangers are presented in Table 2. In addition, experiments were also performed to determine the UA, h_a and $\Delta P/H$ values of these heat exchangers over a range of $\dot{m}_a$.

A compact heat exchanger design is essential when space is constrained. Therefore, while the design aims to increase heat transfer capacity, a reduction in the heat exchanger volume is desired. The volumetric heat flux density ($\dot{q}_v$) of the heat exchanger is a parameter which is often used to evaluate its compactness. As shown in Eq. (11), $\dot{q}_v$ is equal to the overall thermal conductance per unit volume of the heat exchanger. This parameter is similar to that defined by Shah and Sekulić [38] and Unger et al. [15]. Figure 11 shows a comparison of the $\dot{q}_v$ values of the porous lattice and the fin-tube heat exchangers over the range of $\dot{m}_a$ tested. Due to the smaller fin pitch (f_p) of Fin-tube 2 as compared to Fin-tube 1, a greater number of fins can be packed into the heat exchanger at a fixed volume. This resulted in the significantly higher $\dot{q}_v$ of Fin-tube 2 as compared to Fin-tube 1 between the $\dot{m}_a$ values of 0.37 kg/s and 0.78 kg/s. In addition, it can also be observed that between the $\dot{m}_a$ values of 0.37 kg/s and 0.42 kg/s, the porous lattice heat exchangers have higher $\dot{q}_v$ values as compared to the fin-tube heat exchangers. The higher $\dot{q}_v$ values of the lattice heat exchangers are mainly due to the high packing density of the Rhombi-Octet unit cell. Amongst the entire range of $\dot{m}_a$ tested, the highest $\dot{q}_v$ value of 72.1 kW/m^3·K was achieved by Lattice 1 at $\dot{m}_a$ of 0.27 kg/s.

$$\dot{q}_v = \frac{UA}{L \times W \times H} = \frac{UA}{Vol} \tag{11}$$

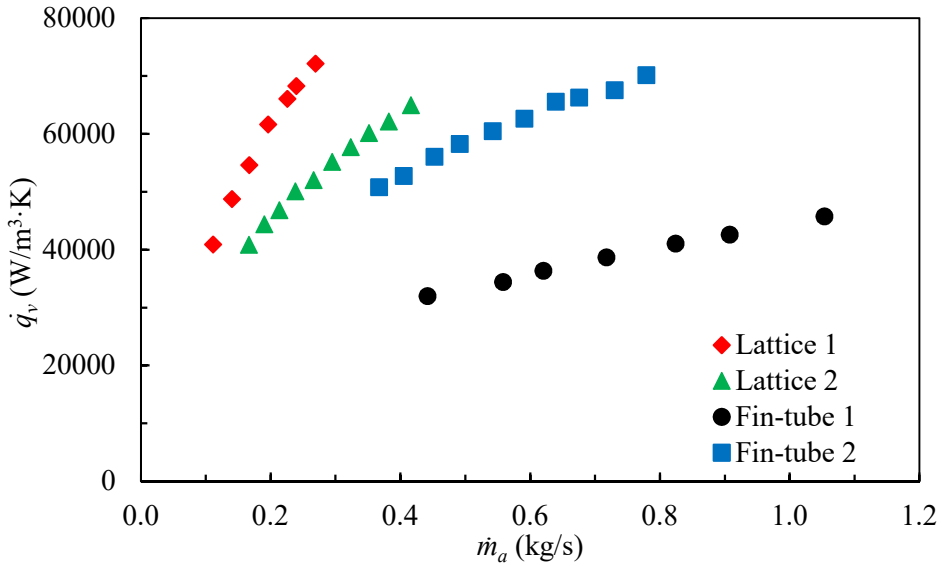

Fig. 11 Comparison of volumetric heat flux densities ($\dot{q}_v$) of porous lattice and fin-tube heat exchangers.

Using the experimental R_a values, the air-side heat transfer coefficients (h_a) of the fin-tube heat exchangers were also computed. In order to obtain h_a, the fin efficiency (η_f) needs to be known. The method of determining η_f of the fin-tube heat exchangers was proposed by Schmidt [39] and employed by Wang et al. [40] and Tang et al. [3]. This method is adopted for the present study to compute h_a of the fin-tube heat exchangers. A detailed explanation of Schmidt's method [39] is presented in Appendix A. Figure 12 shows a comparison of the h_a values of the porous lattice and the fin-tube heat exchangers. It can be seen that between the $\dot{m}_a$ values of 0.37 kg/s and 0.42 kg/s, the porous lattice structures produced significantly higher h_a values than the fin-tube configurations. For example, at $\dot{m}_a$ of approximately 0.37 kg/s, the h_a value of Lattice 2 is about 2.72 times that of Fin-tube 2. The high heat transfer coefficient of the lattice structures is most likely due to the presence of interconnected pores which enhances air mixing. In addition, the ligaments of the lattice structure may have also caused large disturbance to the air flow and produced eddies downstream of the ligaments. This phenomenon was also reported in Ref. [10] and may have further enhanced h_a.

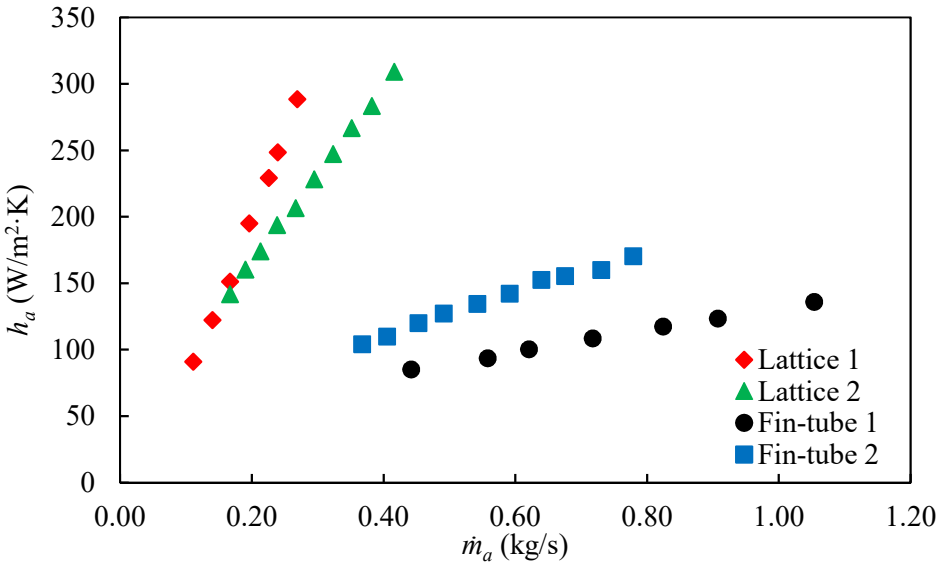

Fig. 12 Comparison of air-side heat transfer coefficients (h_a) of porous lattice and fin-tube heat exchangers.

Even though the porous lattice heat exchangers demonstrated significant enhancements in the air-side heat transfer coefficients, the pressure drops across these heat exchangers are also high. Therefore, for practical

applications, it is essential to consider the pumping power ($\dot{W}$) required to achieve the heat transfer coefficient (h_a). In the following analysis, the pumping power per unit depth of the heat exchanger ($\dot{W}/H$) is considered and it is computed by Eq. (12). It should be noted that even though it is not presented, the pressure drops across the fin-tube heat exchangers were also measured and their $\dot{W}/H$ values were computed. A comparison of the heat exchangers' h_a values over the range of $\dot{W}/H$ tested is shown in Fig. 13. It can be seen that at the same pumping power, both porous lattice heat exchangers have similar h_a and the same trend is observed for the fin-tube heat exchangers. At low $\dot{W}/H$, the porous lattice and fin-tube heat exchangers have similar h_a values. However, with the increase in $\dot{W}/H$, significantly higher h_a values are achieved by the porous lattice heat exchangers and the enhancements in h_a are about 45% as compared to the fin-tube heat exchangers.

$$\frac{\dot{W}}{H} = \frac{V_a \Delta P}{H} \tag{12}$$

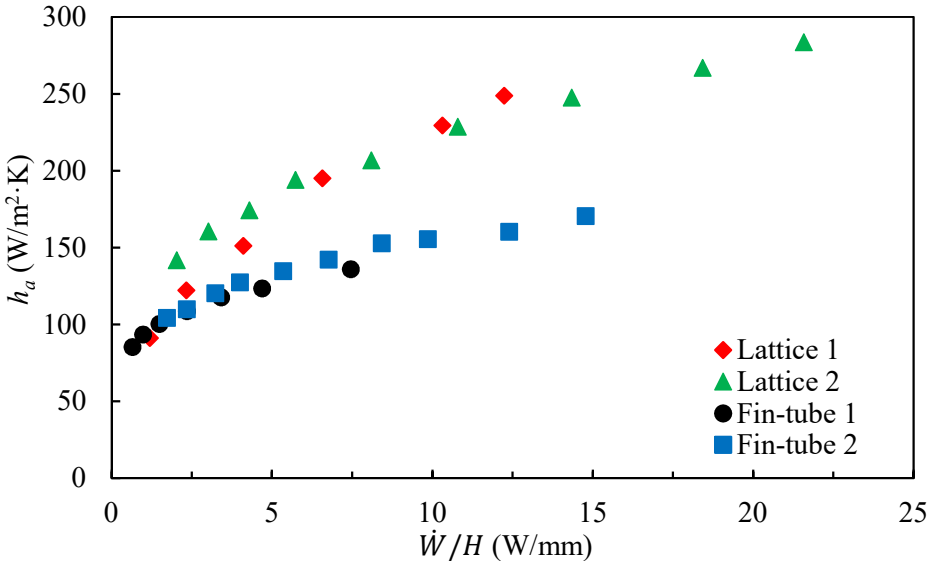

Fig. 13 Comparison of air-side heat transfer coefficients (h_a) at various pumping power per unit depth ($\dot{W}/H$) of porous lattice and fin-tube heat exchangers.

Fig. 14 shows a comparison of the air-side heat transfer coefficients (h_a) of heat exchangers at various pressure drops ($\Delta P/H$). Due to the limited range of ΔP of the fin-tube heat exchangers tested in our investigation, a trend line is applied to estimate their h_a values at higher $\Delta P/H$. This method of analysis was similarly reported by Chumpia and Hooman [24, 25] and is adopted in this analysis. In addition, the trend line of the lattice heat exchanger is also plotted in Fig. 14 and both trend lines are shown in dotted lines. It can be seen from the figure that at lower $\Delta P/H$, the fin-tube heat exchangers exhibit slightly higher h_a than the lattice heat exchangers. However, above $\Delta P/H$ of 0.0275 kPa/mm, the h_a values of the lattice heat exchangers increase significantly and surpass those of the fin-tube heat exchangers. This comparison, therefore, suggests that the lattice heat exchangers should be operated above the $\Delta P/H$ value of 0.0275 kPa/mm to take advantage of their high h_a values.

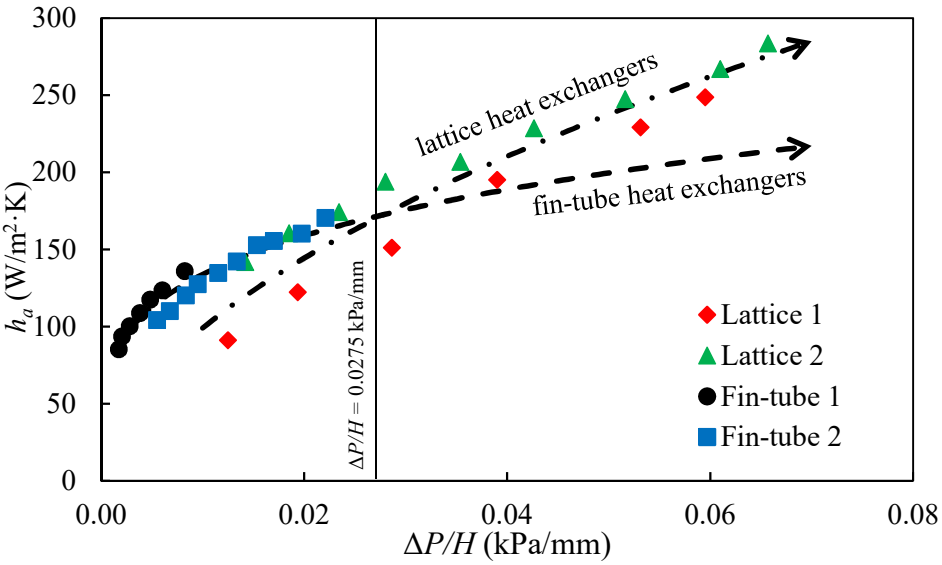

Fig. 14 Comparison of air-side heat transfer coefficients (h_a) at various pressure drop per unit depth ($\Delta P/H$) of porous lattice and fin-tube heat exchangers.

The air-side Reynolds number (Re_a) and Nusselt number (Nu_a) defined by Eqs. (13) and (14), respectively are the other parameters that are commonly used to evaluate the performance of the heat exchangers. It should be noted that in Eqs. (13) and (14), D_h denotes the hydraulic diameter of a heat exchanger and is given by Eq. (15), where A_c is the minimum cross-sectional free flow area of the heat exchanger. This method of computing D_h was also employed by previous investigators in Refs. [1, 27, 41] for different types of heat exchangers.

$$\mathrm{Re}_a = \frac{\rho_a u_a D_h}{\mu_a} \tag{13}$$

$$\mathrm{Nu}_a = \frac{h_a D_h}{k_a} \tag{14}$$

$$D_h = \frac{4A_c H}{A_a} \tag{15}$$

A comparison of the Nu_a values of the heat exchangers at various Re_a is shown in Fig. 15. It can be seen from the present investigation that Re_a ranges from 500 to 4000 and both the lattice and the fin-tube heat exchangers have a similar range of Re_a. In addition, for the range of Re_a that is common to all lattice and fin-tube heat exchangers, the Nu_a values of the lattice heat exchangers are consistently higher than those of the fin-tube heat exchangers. This comparison further confirms the superior air-side heat transfer performance of the lattices structures as compared to conventional fin designs. Finally, it should be noted that many existing studies such as those of Refs. [1, 27, 41] focused mainly on investigating the thermal performances of heat exchangers for $\mathrm{Re}_a \leq 2000$. The larger range of Re_a in the present investigation, therefore, provides new data that can be useful for the design of heat exchangers for high air flow applications.

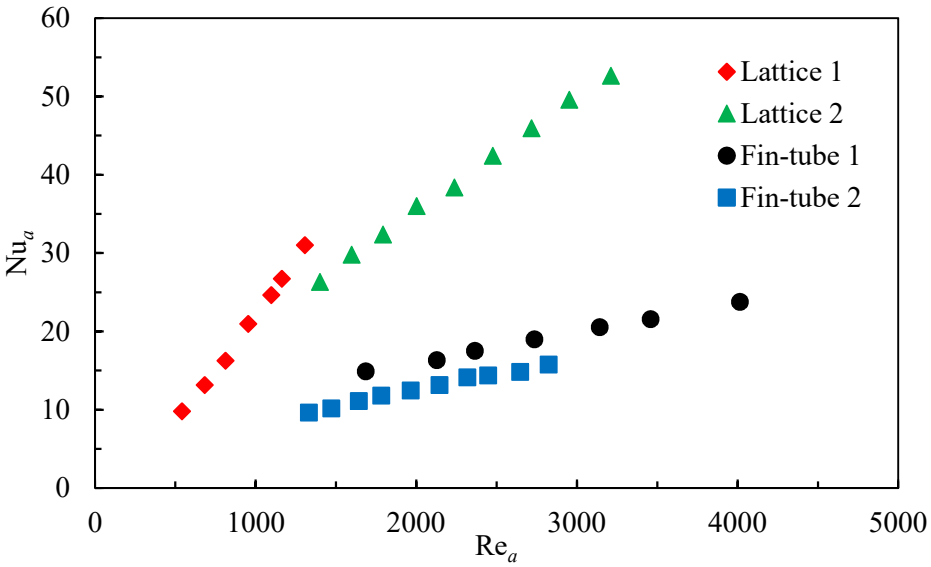

Fig. 15 Comparison of air-side Nusselt numbers (Nu_a) at various Reynolds numbers (Re_a) of porous lattice and fin-tube heat exchangers.

5. Conclusions

In this investigation, two commercial-scale porous lattice heat exchangers of different lattice unit cell sizes were fabricated by selective laser melting (SLM). Experiments were performed in a wind tunnel to characterize the thermal-hydraulic performances of the heat exchangers. The thermal performance indicators such as the overall thermal conductance (UA), air-side thermal resistance (R_a), heat transfer coefficient (h_a) and volumetric heat flux density ($\dot{q}_v$) of the porous lattice heat exchangers were determined and comparisons were made against two conventional fin-tube heat exchangers (Fin-tube 1 and Fin-tube 2). Based on our experimental results and analysis, the following conclusions can be drawn:

1. A comparison of the porous lattice heat exchangers showed that Lattice 1 exhibited approximately 40 – 45% higher UA and h_a than Lattice 2. However, the pressure drop across Lattice 1 was also higher than that of Lattice 2.

2. Due to the high packing density of the porous lattice arrangements, the volumetric heat flux density ($\dot{q}_v$) of the porous lattice heat exchangers were found to be consistently higher than those of the fin-tube heat exchangers for the entire range of $\dot{m}_a$ tested.

3. At the same $\dot{m}_a$, the h_a values of the porous lattice exchangers were more than 2 times those of the fin-tube heat exchangers whereas at the same $\dot{W}/H$, the porous lattice heat exchangers showed about 45% higher h_a as compared to the fin-tube heat exchangers.

4. The significantly higher h_a of the porous lattice as compared to the fin-tube heat exchangers was mainly attributed to the presence of interconnected pores in the porous matrix and the formation of eddies downstream of the ligaments that improved fluid mixing.

These results demonstrated the potential of using SLM to fabricate commercial-scale heat exchangers with enhanced heat transfer performances.

Acknowledgements

The SLM 250 equipment used in this research is supported by the National Research Foundation, Prime Minister's Office, Singapore under its Medium-Sized Centre funding scheme. The authors would also like to acknowledge Dr. K.K. Wong for his assistance during the fabrication stage of the porous lattice heat exchangers.

Appendix A – Determination of fin efficiency (n_f) of the fin-tube heat exchangers

The fin efficiency (η_f) is calculated using an approximation method by Schmidt [39] given by Eq. (A1). In Eqs. (A2) and (A3), r_c represents the fin collar outer radius, k_f is the thermal conductivity of the aluminum fins and f_t denotes the fin thickness. In this study, r_c is taken as the sum of the outer tube radius and the aluminum fin thickness.

$$\eta_f = \frac{\tanh(m_f r_c \emptyset)}{m_f r_c \emptyset} \tag{A1}$$

where

$$m_f = \sqrt{\frac{2h_a}{k_f f_t}} \tag{A2}$$

$$\emptyset = \left(\frac{R_{eq}}{r_c} - 1\right)\left[1 + 0.35 \ln \frac{R_{eq}}{r_c}\right] \tag{A3}$$

Since the heat exchangers are arranged in a staggered layout, the expression for R_{eq} is given by Eq. (A4).

$$\frac{R_{eq}}{r_c} = 1.27 \frac{X_M}{r_c}\left(\frac{X_L}{X_M} - 0.3\right)^{1/2} \tag{A4}$$

where

$$X_L = 0.5\sqrt{\left(\frac{Z_T}{2}\right)^2 + (Z_L)^2} \tag{A5}$$

$$X_M = \frac{Z_T}{2} \tag{A6}$$

In Eqs. (A5) and (A6), Z_T and Z_L denote the transverse and longitudinal tube pitches and are depicted schematically in Fig. A1. By using Eqs. (7), (8) and (A1) – (A6), the air-side heat transfer coefficient (h_a) of the fin-tube heat exchangers can be determined through an iterative process.

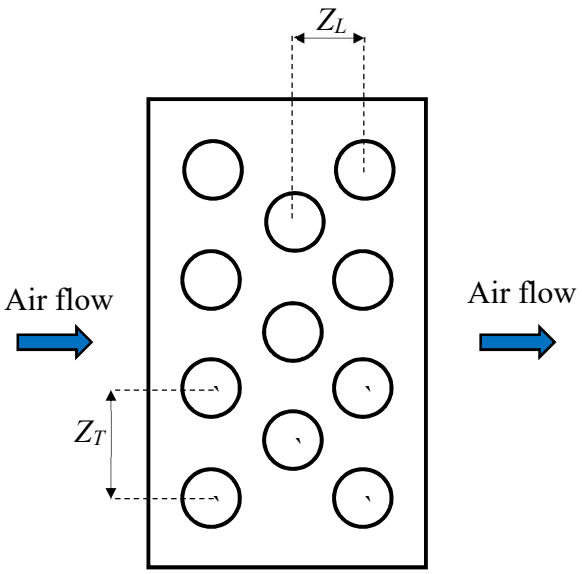

Fig. A1 Details of fin and tube configuration.

References

[1] Wang, C.-C., Lee, W.-S., Sheu, W.-J., A comparative study of compact enhanced fin-and-tube heat exchangers, Int. J. Heat Mass Transf. 44 (2001) 3565-3573.
[2] Wang, C.-C., Hwang, Y.-M., Lin, Y.-T., Empirical correlations for heat transfer and flow friction characteristics of herringbone wavy fin-and-tube heat exchangers, Int. J. Refrig. 25 (2002) 673-680.
[3] Tang, L.H., Zeng, M., Wang, Q.W., Experimental and numerical investigation on air-side performance of fin-and-tube heat exchangers with various fin patterns, Exp. Therm. Fluid Sci. 33 (2009) 818-827.
[4] Wen, M.-Y., Ho, C-Y., Heat-transfer enhancement in fin-and-tube heat exchanger with improved fin design, Appl. Therm. Eng. 29 (2009) 1050-1057.
[5] He, J., Liu, L., Jacobi, A.M., Air-side heat-transfer enhancement by a new winglet-type vortex generator array in a plain-fin round-tube heat exchanger, J. Heat Transf. 132 (2010) 071801-1-071801-9.
[6] Wang, C.-C., Chen, K.-Y., Lin, Y.-T., Investigation of the semi-dimple vortex generator applicable to fin-and-tube heat exchangers, Appl. Therm. Eng. 88 (2015) 192-197.
[7] Wang, C.-C., Chen, K.-Y., Liaw, J.-S., Tseng, C.-Y., An experimental study of the air-side performance of fin-and-tube heat exchangers having plain, louver, and semi-dimpled vortex generator configuration, Int. J. Heat Mass Transf. 80 (2015) 281-287.
[8] Fasano, M., Ventola, L., Calignano, F., Manfredi, D., Ambrosio, E.P., Chiavazzo, E., Asinari, P., Passive heat transfer enhancement by 3D printed Pitot tube based heat sink, Int. Commun. Heat Mass Transf. 74 (2016) 36-39.
[9] Kirsch, K.L., Thole, K.A., Pressure loss and heat transfer performance for additively and conventionally manufactured pin fin arrays, Int. J. Heat Mass Transf. 108 (2017) 2502-2513.
[10] Son, K.N., Weibel, J.A., Kumaresan, V., Garimella, S.V., Design of multifunctional lattice-frame materials for compact heat exchangers, Int. J. Heat Mass Transf. 115 (2017) 619-629.
[11] Alexandersen, J., Sigmund, O., Meyer, K.E., Lazarov, B.S., Design of passive coolers for light-emitting diode lamps using topology optimisation, Int. J. Heat Mass Transf. 122 (2018) 138-149.
[12] Arie, M.A., Shooshtari, A.H., Rao, V.V., Dessiatoun, S.V., Ohadi, M.M., Air-side heat transfer enhancement utilizing design optimization and an additive manufacturing technique, J. Heat Transf. 139 (2017) 031901-1-031901-12.
[13] Arie, M.A., Shooshtari, A.H., Ohadi, M.M., Experimental characterization of an additively manufactured heat exchanger for dry cooling of power plants, Appl. Therm. Eng. 129 (2018) 187-198.
[14] Zhang, X., Tiwari, R., Shooshtari, A.H., Ohadi, M.M., An additively manufactured metallic manifold-microchannel heat exchanger for high temperature applications, Appl. Therm. Eng. 143 (2018) 899-908.
[15] Unger, S., Beyer, M., Gruber, S., Willner, R., Hampel, U., Experimental study of the air-side thermal-flow performance of additively manufactured heat exchangers with novel fin designs, Int. J. Therm. Sci. 146 (2019) Article 106074.
[16] Greiciunas, E., Borman, D., Summers, J., Smith, S.J., A numerical evaluation of next generation additive layer manufactured inter-layer channel heat exchanger, Appl. Therm. Eng. 162 (2019) Article 114304.
[17] Hathaway, B.J., Garde, K., Mantell, S.C., Davidson, J.H., Design and characterization of an additive manufactured hydraulic oil cooler, Int. J. Heat Mass Transf. 117 (2018) 188-200.
[18] Saltzman, D., Bichnevicius, M., Stephen, L., Simpson, T.W., Reutzel, E.W., Dickman, C., Martukanitz, R., Design and evaluation of an additively manufactured aircraft heat exchanger, Appl. Therm. Eng. 138 (2018) 254-263.
[19] Boomsma, K., Poulikakos, D., Zwick, F., Metal foams as compact high performance heat exchangers, Mech. Mater. 35 (2003) 1161-1176.
[20] Leong, K.C., Jin, L.W., Effects of oscillating frequency on heat transfer in metal foam heat sinks of various pore densities, Int. J. Heat Mass Transf. 49 (2006) 671-681.
[21] Ribeiro, G.B., Barbosa Jr., J.R., Prata, A.T., Performance of microchannel condensers with metal foams on the air-side: application in small-scale refrigeration systems, Appl. Therm. Eng. 36 (2012) 152-160.
[22] Chen, K.-C., Wang, C.-C., Performance improvement of high powered liquid-cooled heat sink via non-uniform metal foam arrangement, Appl. Therm. Eng. 87 (2015) 41-46.

[23] T'Joen, C., De Jaeger, P., Huisseune, H., Van Herzeele, S., Vorst, N., De Paepe, M., Thermo-hydraulic study of a single row heat exchanger consisting of metal foam covered round tubes, Int. J. Heat Mass Transf. 53 (2010) 3262-3274.
[24] Chumpia, A., Hooman, K., Performance evaluation of tubular aluminium foam heat exchangers in single row arrays, Appl. Therm. Eng. 83 (2015) 121-130.
[25] Chumpia, A., Hooman, K., Performance evaluation of single tubular aluminium foam heat exchangers, Appl. Therm. Eng. 66 (2014) 266-273.
[26] Nawaz, K., Bock, J., Jacobi, A.M., Experimental studies to evaluate the use of metal foams in highly compact air-cooling heat exchangers, 13th *International Refrigeration and Air Conditioning Conference*, Paper 1283, July 2012, Purdue University Lafayette, Indiana, USA.
[27] Nawaz, K., Bock, J., Jacobi, A.M., Thermal-hydraulic performance of metal foam heat exchanger under dry operating conditions, Appl. Therm. Eng. 119 (2017) 222-232.
[28] Dai, Z., Nawaz, K., Park, Y., Chen, Q., Jacobi, A.M., A comparison of metal-foam heat exchangers to compact multilouver designs for air-side heat transfer applications, Heat Transf. Eng. 33 (2012) 21-30.
[29] Ho, J.Y., Leong, K.C., Cylindrical porous inserts for enhancing the thermal and hydraulic performance of water-cooled cold plates, Appl. Therm. Eng. 121 (2017) 863-878.
[30] Ho, J.Y., Leong, K.C., Enhanced thermal performance of a water-cooled cold plate with porous inserts fabricated by Selective Laser Melting, *Proceedings of the* 13*th International Conference on Heat Transfer, Fluid Mechanics and Thermodynamics* (*HEFAT*2017), 17 – 19 July, Portorož, Slovenia, pp. 860 – 865 (2017).
[31] Ho, J.Y., Leong, K.C., Wong, T.N., Experimental and numerical investigation of forced convection heat transfer in porous lattice structures produced by selective laser melting, Int. J. Therm. Sci. 137 (2019) 276-287.
[32] Bossel, H.H., Computation of axisymmetric contraction, AIAA J. 7 (1967) 2017-2020.
[33] Lam, K., Pomfret, M.J., Design and performance of a low speed wind tunnel, Int. J. Eng. Educ. 13 (1984) 161-172 (1984).
[34] ASHRAE Standard 111-1988 - Practices for measurement, testing, adjusting and balancing of building heating, ventilation air-conditioning, and refrigeration systems, American Society of Heating, Refrigeration and Air-conditioning Engineers, Inc. (1988).
[35] Çengel, Y.A., Ghajar, A.J., Heat and Mass Transfer: Fundamentals and Applications, fifth ed., McGraw-Hill Education, New York, USA, 2015.
[36] Rose, J.W., Heat-transfer coefficients, Wilson plots and accuracy of thermal measurements, Exp. Therm. Fluid Sci. 28 (2004) 77-86.
[37] Moffat, R.J., Using uncertainty analysis in the planning of an experiment, J. Fluids Eng. 107 (1985) 173-178.
[38] Shah, R.K., Sekulić, D.P., Fundamentals of Heat Exchanger Design, John Wiley & Sons, Inc., Hoboken, New Jersey, USA, 2003.
[39] Schmidt, T.E., Heat transfer calculations for extended surfaces, Refrigerating Eng. 57 (1949) 351-357.
[40] Wang, C.-C., Webb, R.L., Chi, K.-Y., Data reduction of air-side performance of fin-and-tube heat exchangers, Exp. Therm. Fluid Sci. 21 (2000) 218-226.
[41] Huisseune, H., De Schampheleire, S., Ameel, B., De Paepe, M., Comparison of metal foam heat exchangers to a finned heat exchanger for low Reynolds number applications, Int. J. Heat Mass Transf. 89 (2015) 1-9.